



LAWRENCE
LIVERMORE
NATIONAL
LABORATORY

LLNL-JRNL-856205

Stratospheric climate anomalies and ozone loss caused by the Hunga Tonga-Hunga Ha'apai volcanic eruption

X. Wang, W. Randel , Y. Zhu, S. Tilmes, J. Starr, W. Yu, R. Garcia, B. Toon , M. Park , D. Kinnison, A. Bourassa, L. Rieger, J. Li

October 20, 2023

Journal of Geophysical Research - Atmospheres

Disclaimer

This document was prepared as an account of work sponsored by an agency of the United States government. Neither the United States government nor Lawrence Livermore National Security, LLC, nor any of their employees makes any warranty, expressed or implied, or assumes any legal liability or responsibility for the accuracy, completeness, or usefulness of any information, apparatus, product, or process disclosed, or represents that its use would not infringe privately owned rights. Reference herein to any specific commercial product, process, or service by trade name, trademark, manufacturer, or otherwise does not necessarily constitute or imply its endorsement, recommendation, or favoring by the United States government or Lawrence Livermore National Security, LLC. The views and opinions of authors expressed herein do not necessarily state or reflect those of the United States government or Lawrence Livermore National Security, LLC, and shall not be used for advertising or product endorsement purposes.

1 **Stratospheric climate anomalies and ozone loss caused by the Hunga Tonga-Hunga
2 Ha'apai volcanic eruption**

3 **Authors:** Xinyue Wang^{1*}, William Randel², Yunqian Zhu^{3, 4, 5}, Simone Tilmes², Jon Starr²,
4 Wandi Yu^{6, 7}, Rolando Garcia², Owen B. Toon^{1, 4}, Mijeong Park², Douglas Kinnison², Jun
5 Zhang², Adam Bourassa⁸, Landon Rieger⁸, Taran Warnock⁸, Jianghanyang Li^{3, 9}

6 **Affiliation:**

7 ¹Department of Atmospheric and Oceanic Sciences, University of Colorado Boulder, Boulder,
8 CO, USA

9 ²Atmospheric Chemistry Observations & Modeling Laboratory, National Center for Atmospheric
10 Research, Boulder, CO, USA

11 ³Cooperative Institute for Research in Environmental Sciences, University of Colorado Boulder,
12 Boulder, CO, USA

13 ⁴Laboratory for Atmospheric and Space Physics, University of Colorado Boulder, Boulder, CO,
14 USA

15 ⁵Chemical Sciences Laboratory, National Oceanic and Atmospheric Administration, Boulder,
16 CO, USA

17 ⁶Department of Atmospheric and Planetary Sciences, Hampton University, VA, USA

18 ⁷Lawrence Livermore National Laboratory, Livermore, CA, USA

19 ⁸Institute of Space and Atmospheric Studies, University of Saskatchewan, Saskatoon, SK,
20 Canada

21 ⁹Institute of Arctic and Alpine Research, University of Colorado Boulder, Boulder, CO, USA

22 Corresponding author: Xinyue Wang (xinyuew@colorado.edu)

23 **Key Points:**

- 24 • Large-scale stratospheric cooling and circulation changes are observed following the
25 Hunga Tonga-Hunga Ha'apai eruption.
- 26 • Observations show ozone reduction in the Southern Hemisphere wintertime midlatitudes
27 and large springtime Antarctic ozone losses in 2022.
- 28 • A chemistry-climate model can track the plumes and capture observed responses to the
29 volcanic eruption.

31 **Abstract**

32 The Hunga Tonga-Hunga Ha'apai (HTHH) volcanic eruption in January 2022 injected
33 unprecedeted amounts of water vapor (H_2O) and a moderate amount of the aerosol precursor
34 sulfur dioxide (SO_2) into the Southern Hemisphere (SH) tropical stratosphere. The H_2O and
35 aerosol perturbations have persisted during 2022 and early 2023 and dispersed throughout the
36 atmosphere. Observations show large-scale SH stratospheric cooling, equatorward shift of the
37 Antarctic polar vortex and slowing of the Brewer-Dobson circulation. Satellite observations
38 show substantial ozone reductions over SH winter midlatitudes that coincide with the largest
39 circulation anomalies. Chemistry-climate model simulations forced by realistic HTHH inputs of
40 H_2O and SO_2 qualitatively reproduce the observed evolution of the H_2O and aerosol plumes over
41 the first year, and the model exhibits stratospheric cooling, circulation changes and ozone effects
42 similar to observed behavior. The agreement demonstrates that the observed stratospheric
43 changes are caused by the HTHH volcanic influences.

44 **Plain Language Summary**

45 The Hunga Tonga-Hunga Ha'apai (HTHH) submarine volcano ($21^{\circ}S$, $175^{\circ}W$) eruption in
46 January 2022 injected unprecedeted amounts of water vapor (H_2O) as well as moderate
47 amounts of aerosol precursor sulfur dioxide (SO_2) into the stratosphere. The H_2O and aerosol
48 perturbations persisted throughout 2022 and were accompanied by large changes in stratospheric
49 climate and ozone chemistry. We use a chemistry-climate model forced by realistic HTHH
50 inputs of H_2O and SO_2 to simulate these stratospheric changes. The model exhibits temperature,
51 circulation, and ozone anomalies in response to these forcings that are similar to those observed.
52 The agreement demonstrates that the observed anomalies impacts are caused by HTHH volcanic
53 influences.

54

55 **1 Introduction**

56 Global ozone levels are recovering due to reductions of CFCs in the stratosphere as the
57 result of the Montreal Protocol and its amendments. However, natural impacts from wildfires
58 (Solomon et al. 2022; 2023; Strahan et al, 2022; Santee et al. 2022) or from large volcanic
59 eruptions (Stone et al. 2017) can temporarily impact stratospheric ozone. The Hunga Tonga-
60 Hunga Ha'apai (HTHH) submarine volcano erupted on 15th January 2022 and increased the
61 global stratospheric water burden by ~10%, setting a record for the modern satellite era and
62 differentiating itself from previous major volcanic eruptions (Vömel, Evan, and Tully 2022;
63 Khaykin et al. 2022; Millan et al. 2022; Randel et al. 2023). The excess moisture is expected to
64 remain in the stratosphere for several years and could exert a substantial impact on the climate
65 system (Solomon et al. 2010; Li and Newman 2020; Jenkins et al. 2023). A moderate amount of
66 sulfur-containing gases, approximately 0.4-0.5 Tg sulfur dioxide (SO_2), about thirty times lower
67 than the emission from Pinatubo (Carn et al. 2022), was lofted into the stratosphere by the
68 HTHH eruption and quickly converted to sulfate aerosol particles (Zhu et al. 2022). Simulations
69 carried out with the Whole Atmosphere Community Climate Model (WACCM), a coupled
70 chemistry-climate model, suggest the excessive moisture halves the SO_2 lifetime and promotes
71 faster sulfate aerosol formation, resulting in large perturbations to stratospheric aerosol evolution
72 (Zhu et al. 2022). As with the H_2O , HTHH aerosols have persisted and dispersed in the SH
73 stratosphere; a notable feature is the separation of the H_2O and aerosol plumes over time due to
74 sedimentation of the aerosols (Legras et al. 2022).

75 It is anticipated that the large H_2O and aerosol perturbations can impact stratospheric
76 temperatures, circulation and chemistry. Substantial stratospheric warming has been observed

77 linked to enhanced aerosols from the eruptions of El Chichón and Pinatubo (e.g., Labitzke and
78 McCormick, 1992; Angell, 1997). While there are no precedents for the large H₂O perturbation
79 in the observational data record, it is expected that increased H₂O will radiatively cool the
80 stratosphere (e.g., Forster and Shine, 1999; Sellitto et al, 2022). Changes to stratospheric ozone
81 (and related trace species) are also expected from large volcanic eruptions due to enhanced
82 aerosol surface areas for heterogeneous chemistry, e.g., Hofmann and Solomon (1989). In this
83 paper we aim to document the observed changes in stratospheric climate and ozone during 2022
84 and early 2023, which are identified as large changes from climatology based on the past two
85 decades. We furthermore run an ensemble of chemistry-climate model simulations using realistic
86 HTHH inputs of H₂O and SO₂ to quantify impacts on stratospheric climate and chemistry, and
87 evaluate their significance compared to internal variability. We first examine the detailed
88 dispersion and evolution of the H₂O and aerosol plumes as observed and as simulated with
89 WACCM to quantify the associated transport and radiative effects. We then compare modeled
90 effects on circulation and ozone with observed anomalies in 2022. Similar behaviors are found in
91 many regards, and these results can be used as fingerprints of HTHH effects on the stratosphere.

92

93 **2 Observational data and model experiments**94 **2.1 Satellite data**

95 a) Microwave Limb Sounder (MLS)

96 The MLS instrument was launched onboard the EOS Aura satellite in 2004 as part of the
97 “A-Train” satellite constellation and has operated continuously since that time in a low-Earth,
98 high-latitude, sun-synchronous orbit. The instrument utilizes five broad microwave spectral

99 regions, with centers ranging approximately from 118 to 2500 GHz, in a limb-viewing
100 configuration to measure various atmospheric properties and constituents, including temperature,
101 H₂O, O₃ and N₂O. For this work, version 5.0 of MLS H₂O, O₃, and temperature data (Waters et
102 al., 2006; Livesey et al., 2020) were compiled into daily zonal means at a resolution of 2.5°
103 latitude. The vertical resolution of temperature changes with pressure, ~3-4 km for 100-10 hPa,
104 ~5-6 km up to 0.01 hPa, and 8-10 km above. The vertical resolution of the H₂O retrievals is ~3
105 km, covering pressure levels 316 hPa to above 1 hPa. Anomalies for 2022 are calculated as
106 deviations from the 2004-2021 background, and we especially highlight anomalies that are
107 outside of all previous variability.

108 b) Ozone Monitor and Profiler Suite Limb Profiler (OMPS-LP)

109 Aerosol extinction and stratospheric aerosol optical depth (sAOD) data are from the
110 University of Saskatchewan (USASK) Ozone Monitor and Profiler Suite Limb Profiler product
111 (Bourassa et al., 2023). These data, derived from a tomographic inversion, provide height-
112 resolved aerosol extinction at 745 nm with a tomographic inversion, with a vertical resolution of
113 1-2 km. The tomographic product improves vertical resolution and reduces artifacts from
114 spatially inhomogeneous aerosols. However, the retrieval relies on assumed aerosol size and
115 optical properties that may cause biases and large uncertainties during periods of enhanced
116 aerosol.

117 **2.2 The fifth generation of European ReAnalysis (ERA5)**

118 Stratospheric circulations are derived using monthly European Center for Medium-Range
119 Weather Forecasts ERA5 reanalysis data on model pressure levels (Hersbach et al., 2020). We
120 include analyses of zonal winds, along with derived residual mean meridional circulation and
121 Eliassen-Palm (EP) fluxes (Andrews, Holton, and Leovy 1987). Anomalies in 2022 are

122 calculated as deviations from the 2004-2021 climatology. We note that the ERA5 assimilation
123 model did not include anomalous stratospheric H₂O or aerosols from HTHH, and hence the
124 model is not balanced and likely incorporates large assimilation increments. This behavior is
125 shown for a different assimilation model in Coy et al. (2022).

126 **2.3 WACCM chemistry-climate model experiments**

127 We use the Community Earth System Model, version 2 (CESM2), with the Whole
128 Atmosphere Community Climate Model (WACCM) (Gettelman et al. 2019) as the atmosphere
129 component, to simulate the stratospheric H₂O and aerosol enhancements due to the HTHH
130 eruption and evaluate their influence on stratospheric temperature, circulation and ozone
131 chemistry. WACCM has 70 vertical layers extending upward to 140 km with vertical resolution
132 of about 1 to 1.5 km in the stratosphere. The model is fully coupled to interactive ocean, sea-ice,
133 and land models, and is initialized at the beginning of January 2022 using the observed sea-
134 surface temperatures following the procedure described in Richter et al. (2022). The HTHH
135 volcanic H₂O (~ 150 Tg) and SO₂ (~0.42 Tg) are injected on January 15, 2022 from ~20 to 35
136 km. The SO₂ injection is tuned based on comparisons between the simulated sulfate aerosol and
137 OMPS Limb Profile aerosol extinction. The H₂O injection is tuned to mimic the observed MLS
138 water vapor profile. More details can be found in Zhu et al. (2022). To accurately simulate the
139 early plume structure and evolution, WACCM winds and temperatures are nudged to the
140 Goddard Earth Observing System (GEOS) Modern-Era Retrospective Analysis for Research and
141 Applications, Version 2 (MERRA-2) meteorological analysis (Gelaro et al. 2017) throughout
142 January 2022; that is, the model is artificially constrained a model by adding a forcing term that
143 relaxes its winds and temperatures towards the MERRA2 data with a 12-hour relaxation time
144 scale. After February 1st, 2022 the model is free-running to simulate fully-coupled variability

145 including the coupling between changes in composition and radiation. We conducted four sets of
146 experiments: the control case without SO_2 or H_2O (no volcanic forcing); an SO_2 only case with
147 only SO_2 injection (with SO_2 converting to sulfate aerosol); an H_2O only case with only H_2O
148 injection, and the $\text{SO}_2+\text{H}_2\text{O}$ case with both SO_2 and H_2O injection, which mimics the total
149 forcing of HTHH eruption. Calculated anomalies are the differences between the forcing runs
150 and the control runs. We include ten ensemble members for each scenario to examine internal
151 variability and to better isolate forced behavior. Individual ensemble members differed by the
152 last date of the meteorological nudging, in the range from 27 January 2022 to 5 February 2022.
153 Once the nudging period ends, the model is free-running.

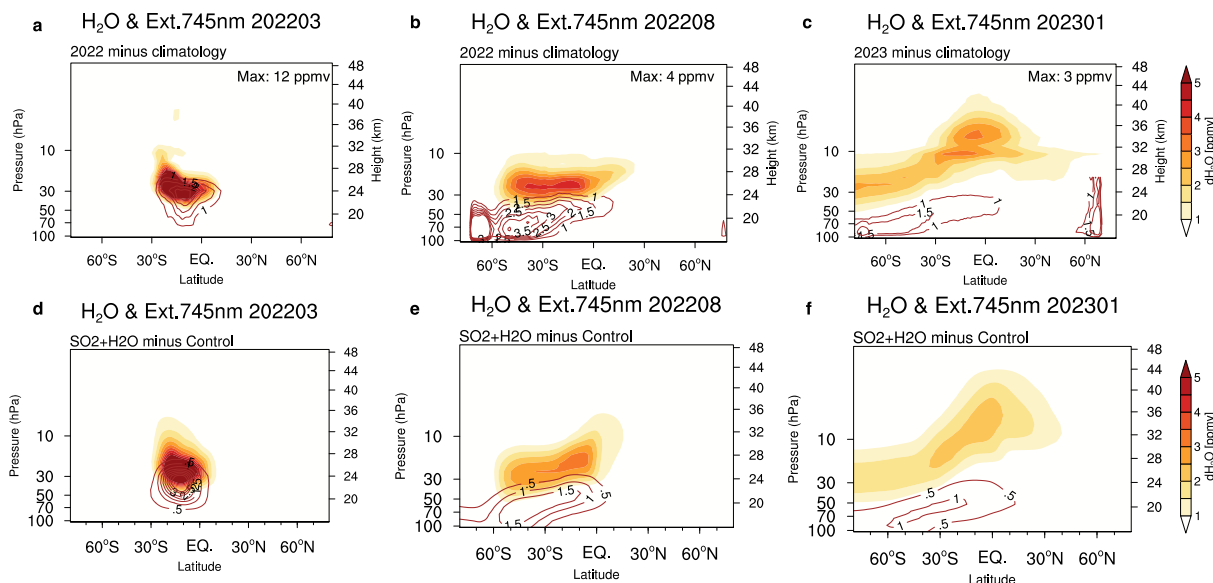
154

155 **3 Results**156 **3.1 Observed and simulated volcanic plumes**

157 Satellite observations show that the HTHH H_2O and aerosol plumes have persisted in the
158 stratosphere and evolved throughout 2022 and early 2023 (Figs. 1a-c). The majority of the
159 sulfate aerosol was initially collocated with the H_2O plume near 24 km (March 2022 in Fig. 1a),
160 but has subsequently sedimented to the lower stratosphere (Legras et al., 2022; Schoeberl et al.,
161 2022) and dispersed in latitude to span much of the Southern Hemisphere (SH) by midwinter
162 (August 2022 in Fig. 1b). As a note, it is unclear from the OMPS extinction measurements in
163 Fig. 1b whether the HTHH aerosols penetrated the Antarctic polar vortex, as the enhanced polar
164 extinction in OMPS-LP measurements is also due to the formation of polar stratospheric clouds
165 in this season. The H_2O plume was centered near 25 km and covered 60°S-20°N by August
166 2022; the H_2O anomalies (>4 ppmv in Fig. 1b and >3 ppmv in Fig. 1c) are large compared to the
167 stratospheric background mixing ratio of ~ 5 ppmv. By January 2023, the H_2O plume ascended in

168 the tropical stratosphere and spread into the Northern Hemisphere midlatitudes (and over the
 169 pole in the SH) while the aerosol layer became weaker and remained over the SH lower
 170 stratosphere (Schoeberl et al. 2023).

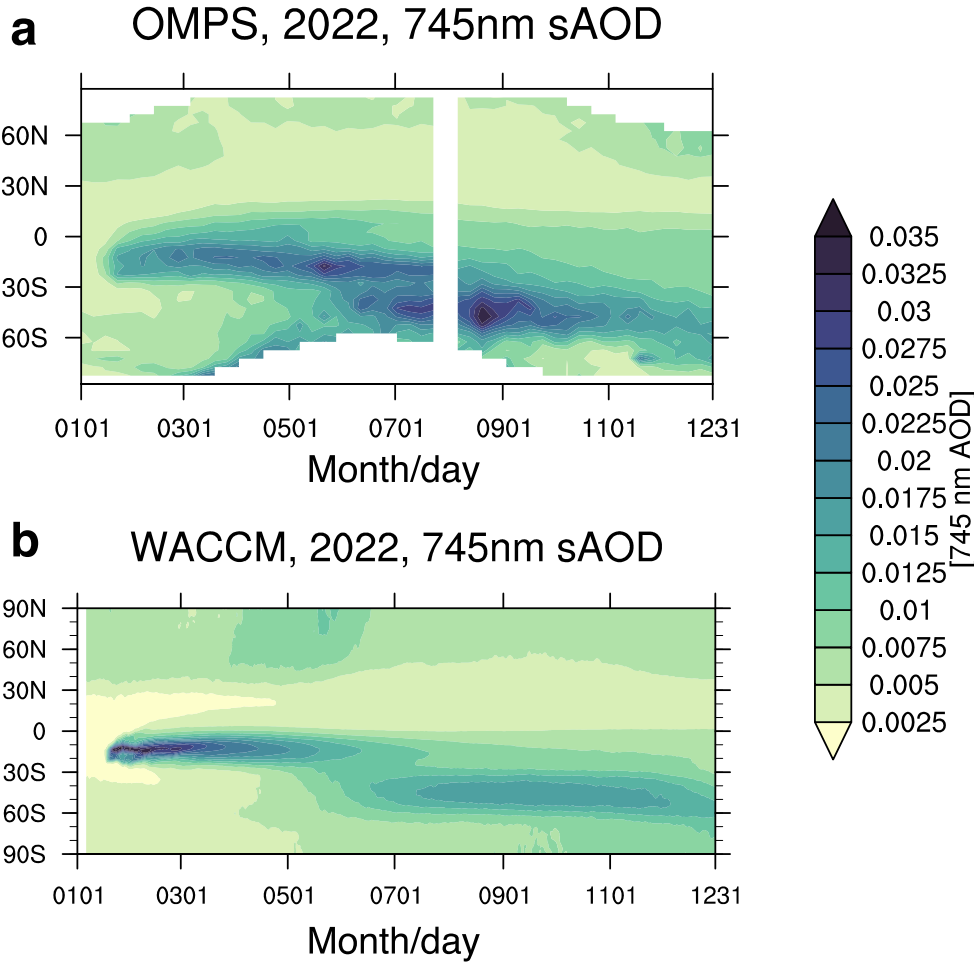
171 The modeled evolution of the H_2O and sulfate aerosol plumes in the $\text{SO}_2+\text{H}_2\text{O}$ case are
 172 shown in Figs. 1d-f, with patterns similar to those observed. Results in Figs. 1d-f are ensemble
 173 averages, but there are relatively small differences in the evolution of the plumes among the 10
 174 realizations (not shown). The H_2O and aerosol plumes initially overlap and then separate
 175 vertically over time, with latitudinal dispersion similar to the observed behavior. The model
 176 HTHH aerosol layer in the lower stratosphere extends to polar latitudes near the bottom of the
 177 polar vortex during winter (Fig. 1e), while the H_2O plume spreads poleward but is mostly
 178 excluded from polar latitudes by the stronger jet near 25 km (see discussion in Section 3.3). The
 179 magnitude of the model aerosol extinction in midwinter is about half as large as measured by
 180 OMPS-LP (cf. Figs. 1b-e), which may be related to uncertainties in SO_2 injection amount and/or
 181 the modeled aerosol size distribution and evolution, along with uncertainties in the OMPS-LP
 182 retrievals.



183

184 **Figure 1.** Observed and simulated H_2O and aerosol perturbations after the HTHH eruption. (a-c)
185 show the observed dispersion of the HTHH H_2O (colors, ppmv) enhancement and aerosol
186 extinction (red contours, 10^{-3} km^{-1}) in (a) March, (b) August 2022 and (c) January 2023.
187 The maximum H_2O amounts are indicated by the number on the top right corner; (d-f) are
188 similar to (a-c) but for WACCM simulations.

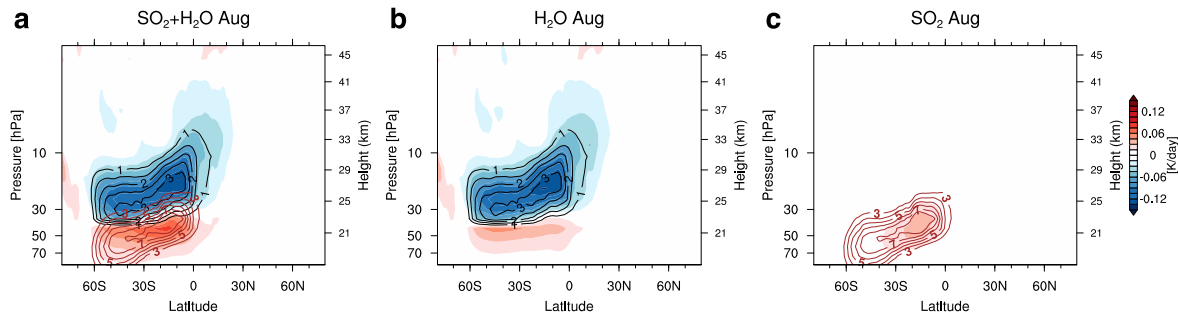
189
190 The HTHH aerosol plume descends over time and disperses meridionally in the SH lower
191 stratosphere. Details of the latitudinal distribution of sAOD observed during 2022 by OMPS are
192 shown in Fig. 2a, suggesting a double-peak sAOD pattern in latitude, with one tropical
193 maximum associated with immediate aerosol formation and one midlatitude maximum during
194 SH winter (~July-September). The double-peak sAOD was also reported from observation and
195 model simulation of the 1991 Pinatubo eruption (Long and Stowe, 1994; Quaglia et al., 2023)
196 and from the response of sustained SO_2 injections under geoengineering (Tilmes et al., 2017).
197 The pattern arises as aerosols spread rapidly across the surf zone into the SH midlatitudes during
198 winter, resulting in a lower sAOD in between. Then the sAOD accumulates in mid-latitudes as
199 the SH polar vortex constitutes a transport barrier. This behavior is qualitatively captured in the
200 WACCM $\text{SO}_2+\text{H}_2\text{O}$ model simulations (Fig. 2b), although the midlatitude sAOD in the model is
201 about half as large as observed. One possible reason is that the model underestimates the aerosol
202 particle effective radius compared with that in SAGE III/ISS (Khaykin et al. 2022) due to either
203 inadequate model microphysics processes or unconsidered pre-existing particles such as sea salt.



205 **Figure 2.** Latitude-time plots of the zonal average stratospheric aerosol optical depth at 745 nm
 206 in 2022 from (a) OMPS-LP and (b) WACCM ensemble $\text{H}_2\text{O}+\text{SO}_2$ ensemble average.
 207 Both panels show total aerosol optical depth, not anomalies.

208
 209 The large perturbations of stratospheric H_2O and aerosol have substantial effects on the
 210 solar and infrared radiation balances, which in turn influence stratospheric temperatures and
 211 circulation. The radiative impacts of H_2O and aerosol volcanic plumes simulated in WACCM are
 212 estimated from the instantaneous radiative heating rates (i.e., longwave heating rate plus
 213 shortwave heating rate, without dynamical or thermal adjustment) due to volcanic plumes, as

214 shown in Fig. 3 for August 2022. Specifically, the water vapor and sulfate aerosols from the
 215 volcanic run are imposed on the no-volcano run, and the shortwave and longwave heating rates
 216 are calculated and output after one model time step, before any thermal or dynamical feedbacks
 217 have occurred. The H_2O plume produces a localized cooling of order -0.1 K/day that overlaps
 218 the plume, while a small heating layer occurs near the bottom due to upwelling longwave
 219 radiation (Fig. 3b). A small net aerosol radiative heating overlaps the aerosol plume (Fig. 3c),
 220 reinforcing the warming below the H_2O plume, so that there is a dipole vertical structure of
 221 cooling above warming for the combined effects (Fig. 3a). The calculated forcings are almost
 222 completely due to longwave effects. Instantaneous radiative heating/cooling rate patterns are
 223 similar in other months (not shown), and decrease slowly over time as the plumes disperse.



224

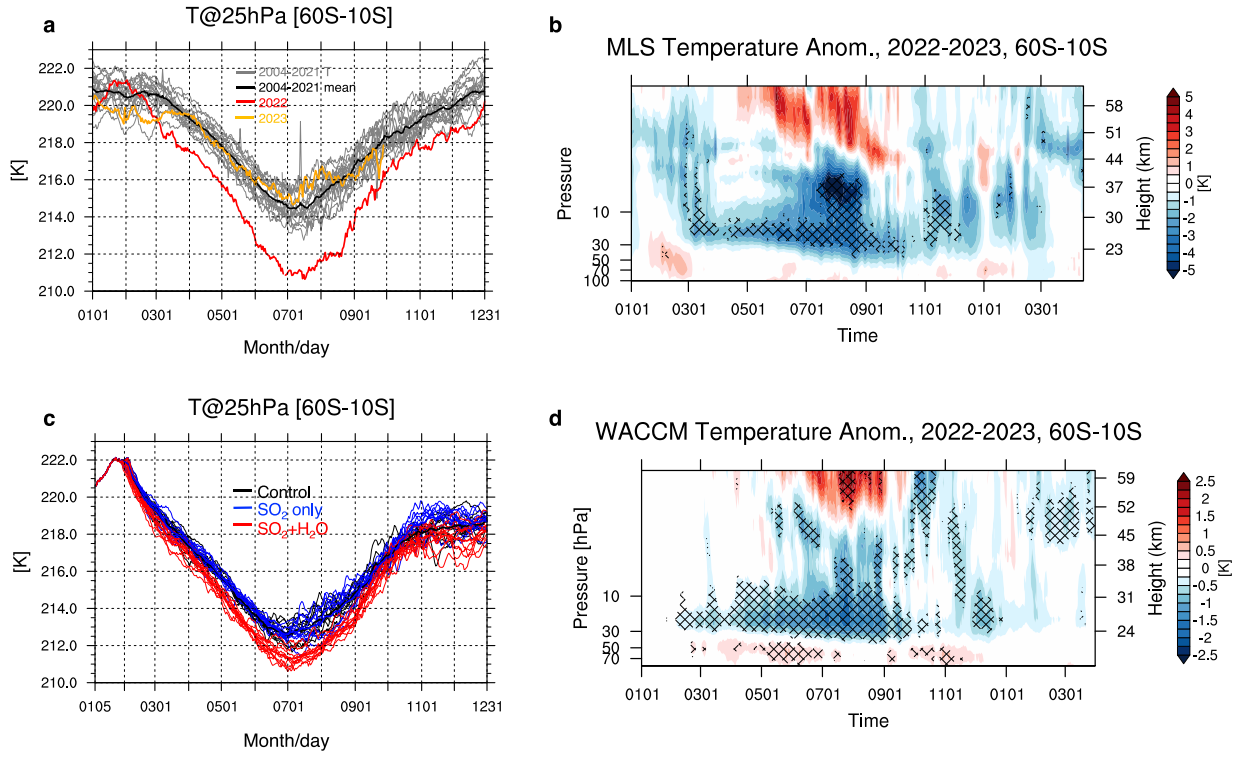
225 **Figure 3.** August net radiative heating rate (longwave plus shortwave tendencies, colors, unit:
 226 K/day) due to (a) both H_2O and aerosol plumes, (b) H_2O plume only, and (c) sulfate
 227 aerosol plume only, compared to no-forcing control runs. Red line contours denote the
 228 sulfate aerosol mixing ratio in ppbv, and black line contours denote the anomalous H_2O
 229 concentration in ppmv.

230 3.2 Temperature perturbation

231 Satellite observations show evidence of systematic stratospheric cooling following the
 232 HTHH eruption (Figs. 4a and b). Temperatures near 25 hPa over the SH show cold anomalies in

233 2022 that are well outside of previous variability, beginning one-to-two months after the eruption
234 (Fig. 4a). This delay is consistent with a radiative response to the increased H₂O near this altitude
235 with a radiative time scale of ~ 10-20 days (e.g. Hitchcock, Shepherd, and Yoden 2010). The
236 vertical structure of the temperature anomalies averaged over 60°S-10°S (Fig. 4b) shows cooling
237 covering much of the mid-stratosphere throughout 2022, with largest cold anomalies during SH
238 winter (June-August) extending to ~45 km. During these months there are anomalous warm
239 temperatures in the lower mesosphere above ~50 km (Yu et al., 2023, see Section 3.3). Cold
240 anomalies are reduced in 2023.

241 The unprecedented evolution of temperatures in 2022 suggests forced changes from the
242 HTHH eruption, but also contains components of internal variability. To evaluate the forced
243 signal in the model runs we use ensemble simulations of WACCM with and without the volcanic
244 injections. The modeled structure of temperature changes in the (H₂O+SO₂) simulations (Figs.
245 4c-d) capture the salient aspects of the observed behavior including cooling throughout the year
246 over ~25-30 km and enhanced winter maxima, including warming in the lower mesosphere (Fig.
247 4d).



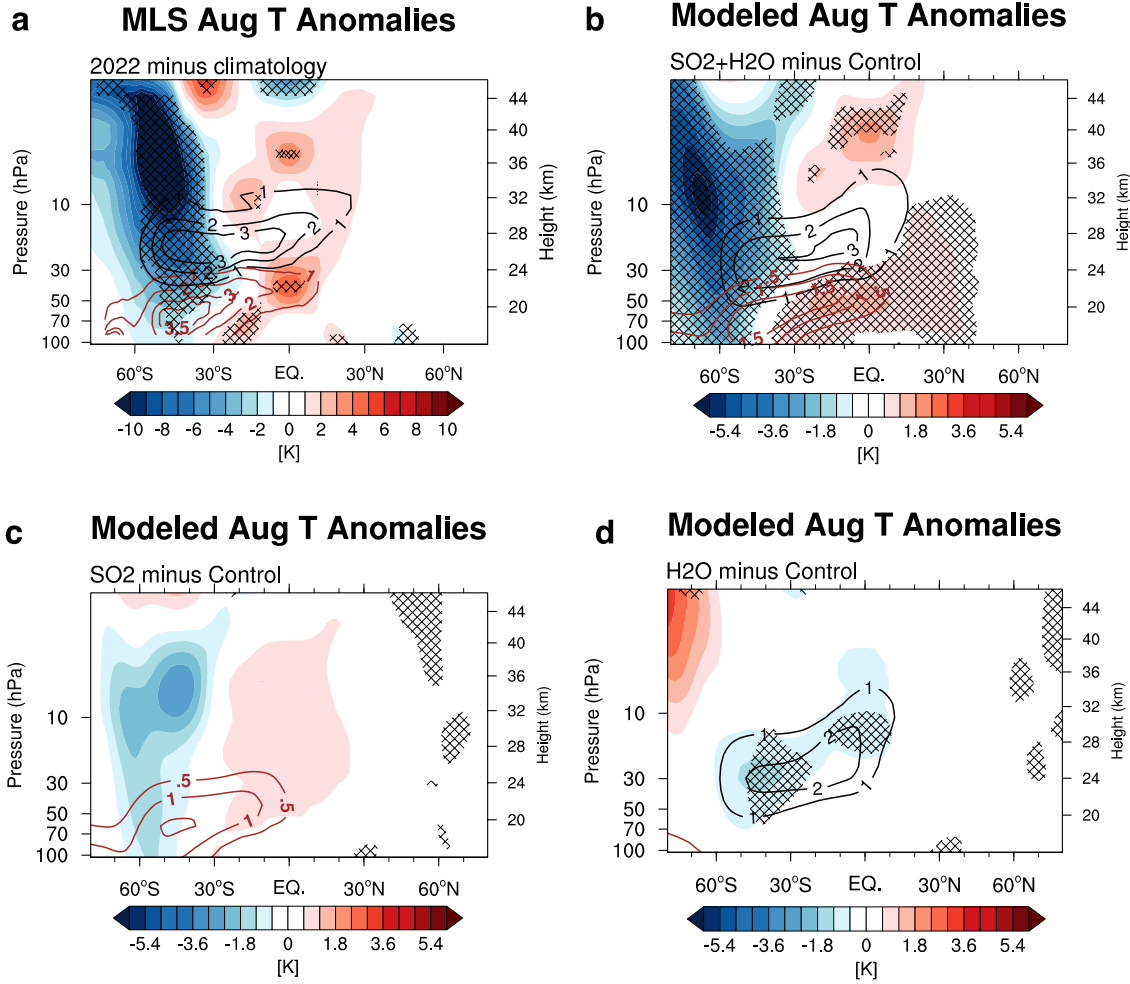
248

249 **Figure 4.** Temperatures averaged over 60°S-10°S from MLS observations showing persistent
 250 anomalous cooling in 2022. (a) Gray lines show time series of MLS temperatures at 25
 251 hPa for 2004-2021 while the black line is the climatology. Red/orange lines shows 25
 252 hPa temperature for 2022/2023. (b) Time-height section of MLS temperature anomalies
 253 (differences from 2004-2021 averages). Hatched regions in (b) indicate where the 2022
 254 anomalies are outside the range of all variability during 2004-2021. (c) As in (a), but
 255 temperatures at 25 hPa simulated in WACCM. Black lines indicate the control cases, blue
 256 lines indicate SO_2 only cases, and red lines indicate the $\text{SO}_2 + \text{H}_2\text{O}$ cases, respectively
 257 (including ten realizations for each case). (d) Time-height section of WACCM
 258 temperature differences for the $\text{SO}_2 + \text{H}_2\text{O}$ minus control ensemble means. Hatched
 259 regions indicate where the temperature anomalies are statistically significant at the 95%

260 level according to Student's *t*-test. Note that color bars in (b) and (d) have different
261 ranges.

262

263 Observed cold temperature anomalies and H₂O plume overlap until April and decouple in
264 early SH winter. The strongest cooling occurs primarily in midlatitudes centered near 50°S, and
265 do not directly overlap the H₂O plume as illustrated for August 2022 in Fig. 6a (other months are
266 shown in Fig. S1). High latitude cold anomalies (in excess of 15 K) occur in combination with
267 warm tropical anomalies, with maxima near 23 and 38 km. Part of the tropical and extratropical
268 temperature maxima are related to the phase of the Quasi-Biennial Oscillation (QBO) in 2022
269 (Coy et al. 2022). The see-saw patterns in temperature (opposite sign responses) between high
270 and low latitudes are suggestive of coupling to the hemispheric-scale mean meridional
271 circulation (Yulaeva, Holton, and Wallace 1994). The strong high latitude temperature anomalies
272 are in balance with changes in the stratospheric circulation, as discussed below.



273

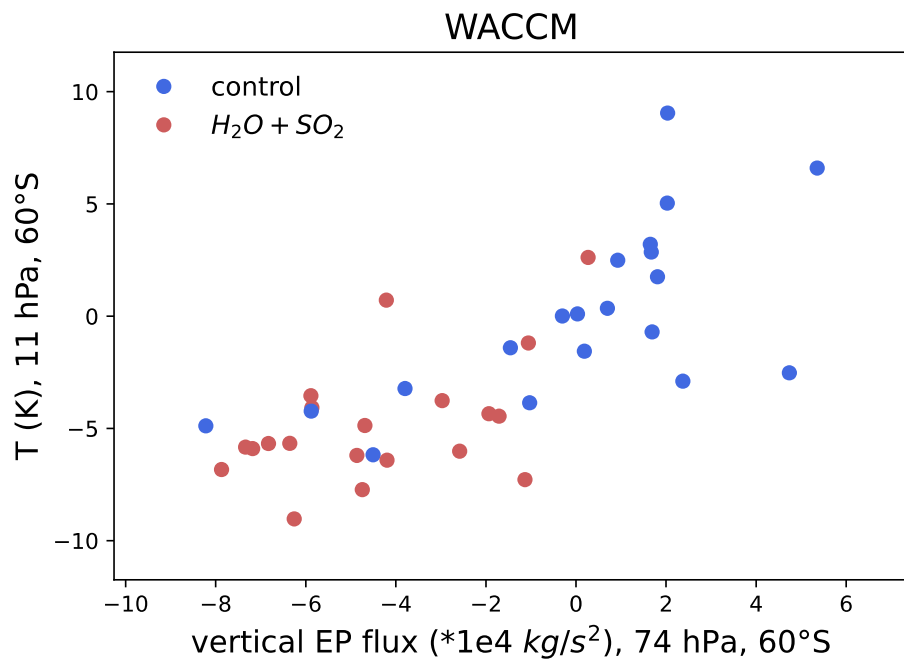
274 **Figure 5.** Observed and modeled temperature anomalies in August 2022 (color shading, K). (a)
 275 MLS observations, calculated as differences between the 2022 and the 2004-2021
 276 average. (b) WACCM simulated modeled temperature changes in the all-forcing
 277 (SO₂+H₂O) case minus the no-forcing control runs. (c) Similar to (b), but for SO₂ only
 278 simulations. (d) Similar to (b), but for H₂O only simulations. Red line contours denote the
 279 sulfate aerosol extinction in 10⁻³ km⁻¹, and black line contours denote the anomalous H₂O
 280 concentration in ppmv. Hatched regions denote statistical significance, as in Fig. 4.

281

282 The simulated ensemble average temperature changes in response to the (SO₂+H₂O)
283 forcing in August are shown in Fig. 5b (other months are shown in Fig. S2); they display patterns
284 similar to observed behavior (Figs. 5a, S1), although the model winter cooling is centered at
285 somewhat higher latitudes (60-70° S). Modeled temperature changes with only SO₂ (sulfate
286 aerosol) forcing (Fig. 5c) have temperature perturbations of similar polarity to the total forcing
287 (tropical warming and high latitude cooling), but are weaker and not significant (see also blue
288 lines in Fig. 4c). Without H₂O injection the volcanic aerosol layer is thicker and heats the lower
289 stratosphere over a deeper vertical layer, implying that the coupled H₂O-aerosol effects have
290 amplified stratospheric cooling in the high latitudes. In contrast, simulations with only H₂O
291 injection show a very different temperature response (Fig. 5d), with weak cooling anomalies in
292 the tropics and midlatitudes that overlap the H₂O plume. The responses due to the single-forcing
293 H₂O and SO₂ perturbations are not additive. Overall, our model sensitivity experiments
294 demonstrate that stratospheric temperature responses change from direct radiative effect in the
295 early stage to much stronger dynamical effect during SH winter. Including both H₂O and SO₂
296 (sulfate aerosol) forcings is important for realistic simulation of the HTHH responses with strong
297 effects only for the combined forcings.

298 The coupling of stratospheric temperature (polar vortex strength) and planetary wave
299 amplitude is a well-known feature of the winter stratosphere, with correlation between wave
300 amplitudes and polar temperature (e.g. Andrews et al., 1987; Holton & Mass, 1976; Randel & Newman,
301 1998). The coupling is evident in Fig. 6 as correlations of polar temperature vs planetary wave
302 activity (quantified as the vertical component of the Eliassen-Palm flux divergence in the lower
303 stratosphere) for our control simulations, showing results for July and August for each of the 10
304 realizations. Figure 6 furthermore shows a systematic shift in temperatures and wave activity in

305 the $\text{H}_2\text{O}+\text{SO}_2$ forced run with respect to the control runs, with colder temperature and weaker
 306 Eliassen-Palm (EP) fluxes associated with the HTHH forcing in most cases. We view this shift as
 307 a fingerprint of the forced response due to the HTHH forcing. While most of the $\text{H}_2\text{O}+\text{SO}_2$
 308 ensemble members show relative cold temperatures and weak wave fluxes, there is considerable
 309 stochastic variability among the realizations, and several realizations (6 out of 10) have
 310 temperature anomalies comparable to the observed 2022 anomalies. We conclude that internal
 311 variability in the ensemble model simulations contributes to the low bias in ensemble average
 312 temperature anomalies in Fig. 4 compared to the observed pattern in 2022 (Yu et al., 2023). In
 313 spite of this difference in magnitude, the similarity in timing and spatial structure of observed
 314 and modeled temperature patterns is strongly suggestive of an HTHH attribution for the observed
 315 anomalies.



316

317 Figure 6. The relationship between temperatures at 60°S , 10 hPa and the vertical component of
 318 EP flux divergence at 60°S , 74 hPa in the WACCM control (blue) and $\text{H}_2\text{O}+\text{SO}_2$ (red)

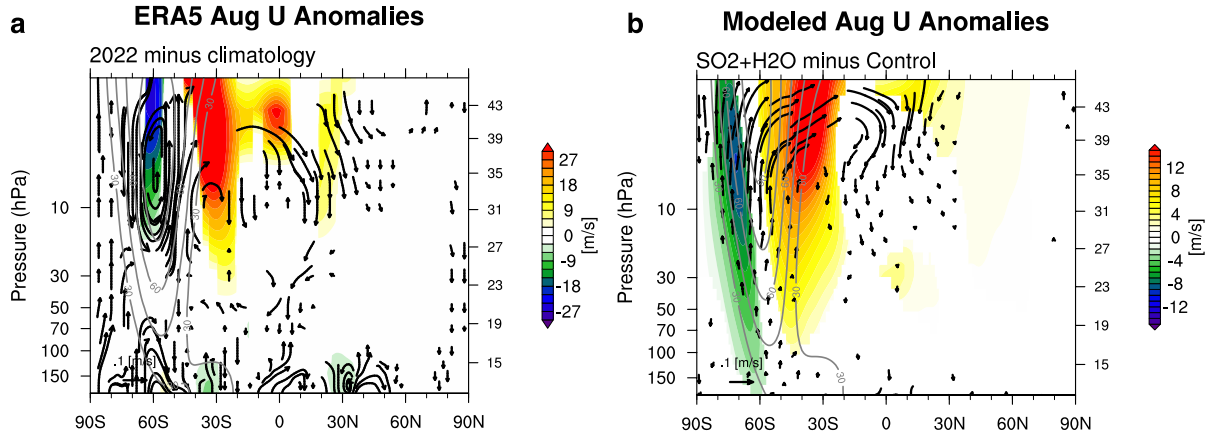
319 simulations. Results are shown for both July and August statistics for the 10 realizations in each
320 ensemble.

321

322 **3.3 Stratospheric circulation response**

323 Because they are in thermal wind balance with the temperature anomalies, the zonal
324 mean zonal winds show intensification and equatorward shift of the polar vortex throughout the
325 winter (see Fig. 7a for August). The simulated zonal wind changes also show a strengthening and
326 equatorward shift of the winter westerlies in response to the (SO₂+H₂O) forcing (Fig. 7b), with
327 patterns similar to the observed anomalies. As with temperatures, the model ensemble mean
328 wind anomalies are only about half as large as observed in 2022. Reanalysis fields and models
329 show that the strengthened polar vortex persists into SH spring (Figs. S3 and S4). Figures 7a-b
330 also include anomalies in the residual mean meridional (Brewer-Dobson) circulation (BDC),
331 highlighting anomalous high latitude upwelling and low latitude downwelling that opposes and
332 weakens the normal background equator to pole circulation. These results are consistent with the
333 residual circulation anomaly patterns discussed in Coy et al. (2022) and the weakened
334 background tropical upward residual circulation in Schoeberl et al. (2022). The changes in the
335 BDC are associated with adiabatic cooling/warming in stratosphere/mesosphere, and are also
336 consistent with weakened planetary-scale wave forcing in the middle and upper stratosphere. As
337 noted above (Fig. 5), the SO₂+H₂O simulations have planetary wave amplitudes and EP fluxes
338 that are about half the size of the control runs, and reanalysis data likewise show weak planetary
339 waves in 2022. We note that the vertical out-of-phase temperature changes above ~50 km
340 observed in winter (Figs. 4b-d) are characteristic of dynamically forced effects, consistent with
341 the reductions in stratospheric EP fluxes (Andrews, Holton, and Leovy 1987). Similar to

342 differences in temperature response (Fig. 6), model simulations with only sulfate aerosol forcing
 343 or only H₂O forcing show mostly insignificant circulation changes (Fig. S5a) or opposite
 344 circulation responses (Fig. S5b) across ten ensembles, highlighting the importance of combined
 345 effects due to sulfate aerosol and H₂O enhancements.



346

347 **Figure 7.** Anomalous zonal wind changes in August 2022. Colors show zonal mean zonal wind
 348 anomalies in (a) observations from the ERA5 reanalysis data and (b) simulations in the
 349 all-forcing (SO₂+H₂O) WACCM simulations compared to the control runs. Gray
 350 contours show the background zonal winds with an interval of 15 m/s. Colored regions in
 351 (a) indicate where the 2022 anomalies are outside the range of all variability during 2004-
 352 2021. The vectors depict anomalies in the residual mean meridional circulation (BDC) in
 353 ERA5 that are outside of two standard deviations. Colored regions and vectors in (b)
 354 indicate where anomalies are significant at the 95% level.

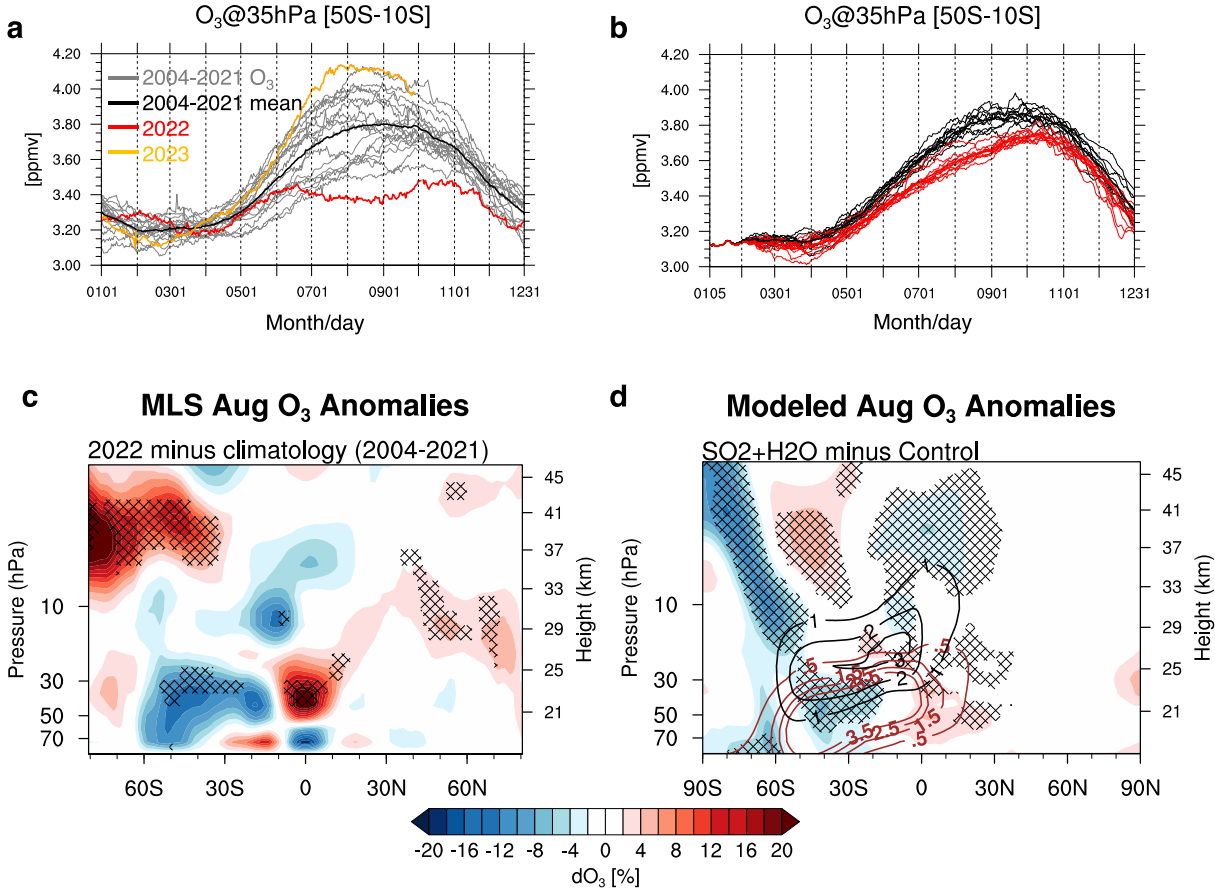
355

356 3.4 Midlatitude stratospheric ozone changes

357 Stratospheric ozone changes after HTHH can be anticipated from both changes in
 358 circulation and anomalous chemistry from enhanced H₂O and aerosols (Tie and Brasseur 1995;

359 Hofmann and Solomon 1989; Solomon 1999; Zhu et al. 2022; Yook, Thompson, and Solomon
360 2022; Lu et al. 2023). MLS observations show lower stratospheric (LS) ozone reductions during
361 winter over the SH midlatitudes and tropics ($\sim 50^{\circ}\text{S}$ - 10°S), which are outside of previous
362 variability (Fig. 8a). The lower stratospheric midlatitude ozone decreases are accompanied by
363 anomalously high values over the equator (Fig. 8c), and part of these coupled anomalies are
364 linked to the phase of the QBO in 2022 ([https://acd-](https://acd-ext.gsfc.nasa.gov/Data_services/met/qbo/qbo.html)
365 [ext.gsfc.nasa.gov/Data_services/met/qbo/qbo.html](https://acd-ext.gsfc.nasa.gov/Data_services/met/qbo/qbo.html)). We note that midlatitude QBO anomalies in
366 ozone often have an asymmetric latitude structure with maximum amplitude in the winter
367 hemisphere (Randel et al., 1999), as observed here. This QBO influence can be seen in the
368 relatively large spread of midlatitude winter ozone amounts in 2004-2021 seen in Fig. 8a, with
369 individual years typically above or below the long-term mean, but note that low values in 2022
370 extend outside of this background variability. The wintertime SH mid-latitude ozone reduction is
371 reproduced in the model (Figs. 8b and d, below 30 hPa), with similar spatial and temporal
372 patterns to those observed, but only about half the anomaly magnitude in the ensemble average.
373 Note the lack of strong interannual variations in the individual model realizations in Fig. 8b, due
374 to a lack of subtropical QBO variability in these idealized model simulations (all 10 realizations
375 are initialized with the same phase of the QBO). The large difference in ozone response between
376 MLS and WACCM in the upper stratosphere (above 30 hPa, poleward of 60°S) is consistent
377 with the streamfunction anomalies shown in Fig. 7, which are computed from the values in 2022
378 minus climatology in MLS and from the 2022 volcano minus no volcano simulations in
379 WACCM.

380



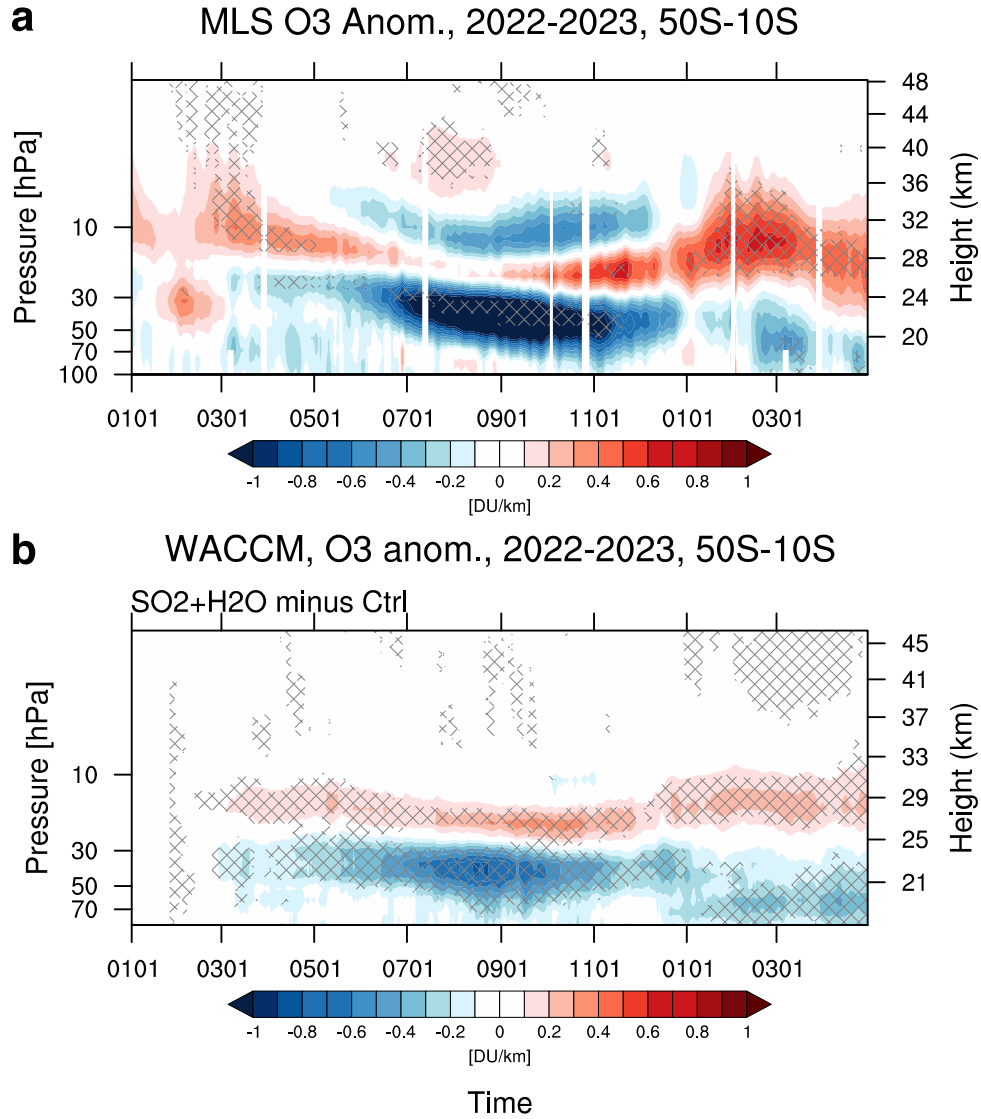
381

382 **Figure 8.** Evolution of midlatitude stratospheric ozone after HTHH. (a) Time series of MLS
 383 observed ozone (in ppmv) at 35 hPa, 50°S-10°S, showing low ozone values in 2022 (red
 384 line) compared to other years. Gray lines show time series for 2004-2021, the black line
 385 is the climatology, and the orange line shows 35 hPa ozone for 2023. (b) Ozone at 35 hPa
 386 simulated in WACCM, comparing the control cases (black lines) and the $\text{SO}_2+\text{H}_2\text{O}$ cases
 387 (red lines). Fractional ozone anomalies (color shading, %) from (c) MLS and (d)
 388 WACCM simulation in August 2022. Regions of significant changes are hatched, as in
 389 Fig. 4.

390

391 The evolution of SH midlatitude ozone changes associated with HTHH is highlighted in
392 Fig. 9, which shows density-weighted ozone anomalies (in DU/km) over 50°-10° S from MLS
393 data and WACCM $\text{SO}_2+\text{H}_2\text{O}$ simulations. Observations show strong negative anomalies in the
394 lower stratosphere that maximize during winter, and similar but weaker patterns are found in the
395 model ensemble mean. There is a narrow layer of ozone increases above the lower level
396 decreases seen in both observations and model in Figs. 8a-b persisting through May 2023. The
397 center or node of this vertical dipole pattern coincides in altitude with the climatological ozone
398 maximum near 25 km, so that these ozone changes are consistent with the weakening of the
399 midlatitude BDC discussed above. The consistency on the timing of circulation changes and LS
400 ozone losses, which both maximize during SH winter (e.g., temperature anomalies in Fig. 4 and
401 ozone losses in Figs. 8-9), is a fingerprint of substantial contribution due to changes in transport.
402 This aligns with the conclusion in Santee et al. (2023) that no appreciable chemical ozone loss
403 occurred in SH midlatitude. We note that while ozone changes in the $\text{SO}_2+\text{H}_2\text{O}$ WACCM
404 simulations result from a combination of transport and chemistry effects, it is not simple to
405 separate dynamical and chemical contributions in our coupled simulation. Complementary
406 studies using Specified Dynamics WACCM (SD-WACCM) may help quantify the importance of
407 the different chemical and dynamical processes affecting the midlatitude ozone loss (Zhang et
408 al., 2023).

409



410

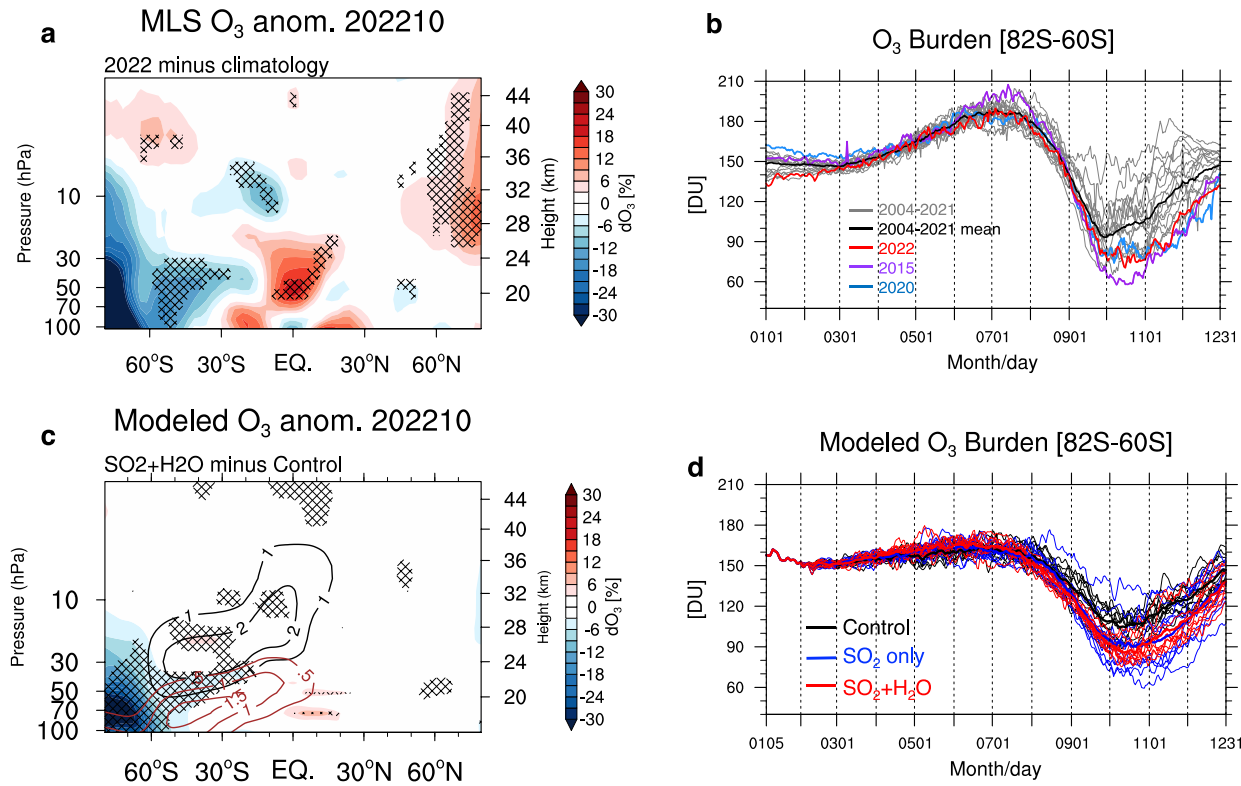
411 **Figure 9.** Time-height sections of ozone density anomalies (units: DU/km) averaged over 10-
 412 50°S, showing results from (a) MLS observations and (b) WACCM model simulations
 413 (ensemble average SO₂+H₂O minus control). Hatched regions denote significance, as in
 414 Fig. 4.

415

416 **4.5 Antarctic stratospheric ozone**

417 Anomalous ozone changes during 2022 are also found associated with the Antarctic
418 ozone hole (Figs. 10a and b), where variability is tied to polar stratospheric cloud (PSC) and
419 aerosol amounts together with cold temperatures that generate photochemically active chlorine
420 (Solomon et al. 1986; Zhu et al. 2017). In the model, springtime polar ozone losses are enhanced
421 by HTHH aerosols that reach the polar stratosphere (red contours in Fig. 10c), in combination
422 with anomalously cold temperatures from circulation effects that enhance reactive chlorine
423 chemistry. The combined effects of $\text{SO}_2 + \text{H}_2\text{O}$ lead to net losses of ~ 15 DU compared to control
424 runs amid substantial variability in the polar region (Fig. 10d), and comparisons with SO_2 only
425 simulations (blue lines in Fig. 10d) show that most of the polar ozone losses are due to the
426 impact of HTHH aerosols. Time series in Fig. 9d show that the ozone loss rates accelerate in
427 September, during the formation of the ozone hole. MLS observations show a relatively deep
428 ozone hole in October 2022 (Figs. 10a-b), but differences with previous years are only apparent
429 during and after October; this detail is different from the model behavior, where differences are
430 already noticeable in September. The bias may come from comparing the anomaly from 2004-
431 2021 climatology versus the anomaly from control runs. We note that, while the HTHH aerosols
432 penetrated across the bottom of the polar vortex and provided more surface area to promote
433 heterogenous chemistry in the model (Fig. 1e), it is unclear if this behavior occurred in the real
434 atmosphere because enhanced polar aerosol extinction in the OMPS data (e.g. Fig. 1b) could
435 simply reflect the occurrence of polar stratospheric clouds. In any case, the observed Antarctic
436 ozone remains near record low levels during SH spring (October-December in Fig. 10b), rivaling
437 other recent years with enhanced polar aerosols due to volcanic eruptions such as the Calbuco
438 volcanic eruption in 2015 (purple line in Fig. 10b, Solomon et al., 2016; Stone et al., 2017; Zhu

439 et al., 2018) and smoke from wildfires (blue line in Fig. 10b, Australian bush fires in 2020
 440 persisting into 2021; Rieger et al., 2021).



441
 442 **Figure 10.** (a) Fractional ozone anomalies (%) from MLS in October 2022. Hatched regions
 443 indicate where the 2022 anomalies are outside the range of all variability during 2004-
 444 2021. (b) MLS observations of polar cap (82°S-60°S) ozone column over 11-22 km in
 445 2004-2022. (c) Similar to (a) but modeled October ozone changes in SO₂+H₂O minus
 446 control simulations. Hatched regions mark the grid points for which the changes exceed
 447 the 95% significance level according to Student's *t*-test. (d) Similar to (b) but
 448 corresponding modeled results comparing control, SO₂+H₂O and SO₂ only simulations.

449
 450 **4. Conclusion**

451 Satellite measurements demonstrate persistent perturbations in stratospheric temperatures
452 and circulation following the HTHH eruption, including influences on the seasonally-evolving
453 polar vortex, planetary waves and Brewer-Dobson circulation. Global chemistry-climate model
454 simulations forced by HTHH inputs can track the evolving H₂O and aerosol plumes, and the
455 modeled volcanic responses in temperatures and circulation in the SH are similar to the time-
456 evolving patterns of the observed behavior. This agreement suggests that the observed
457 stratospheric changes are a fingerprint of the forced global-scale response to the HTHH eruption.
458 Several realizations have strong responses in temperature and circulation as large as that
459 observed in 2022, however, the ensemble average forced model responses are only about half the
460 magnitude of observed anomalies in 2022. These differences are likely related to large stochastic
461 variability due to wave-mean flow coupling during SH winter, evident in model simulations (Fig.
462 6) and are not negligible compared to the HTHH forcing. Comparison of control and HTHH
463 model results (Fig. 6) suggests that the HTHH forcing biases pushed the system towards a
464 balance of weak wave fluxes and a cold/strong polar vortex, although the dynamical details are
465 not well understood. Sensitivity experiments further demonstrate that the combined effects of
466 both H₂O and SO₂ (sulfate aerosol) are important in these simulations, as smaller and
467 insignificant changes are found in individual H₂O or SO₂ forcing experiments.

468 MLS observations show anomalous low ozone in the SH winter midlatitude lower
469 stratosphere following HTHH; although some component of these low values is probably related
470 to the phase of the QBO (as evidenced by out-of-phase changes over the equator), the low 2022
471 values are outside of all previous variability. The WACCM SO₂+H₂O simulations capture the
472 key spatial and temporal patterns of these midlatitude ozone changes, arguing for an HTHH
473 attribution of the observed low values. Large ozone decreases during 2022 are also found

474 associated with the Antarctic ozone hole. While it is not simple to separate ozone changes due to
475 transport and chemistry effects in our coupled model simulations, the spatial and temporal
476 fingerprints suggest a dominant contribution from transport effects at midlatitudes, and from
477 heterogeneous chemistry in the Antarctic. Future studies using models constrained with nudged
478 meteorological fields may help separate the influence of chemistry from dynamics. The
479 WACCM simulations show that aerosol transported to the Antarctic lower stratosphere
480 combined with a circulation-induced cold polar vortex contributed to low Antarctic ozone levels
481 in the model during September-December (i.e., a relatively deep ozone hole). Observed Antarctic
482 ozone levels were relatively low during October-December 2022 (Fig. 10b), consistent with the
483 model behavior, although there is no evidence of anomalous amounts of reactive Cl species
484 inside the vortex (Manney et al., 2023). The 2022 SH ozone losses caused by HTHH are
485 transient effects and should not impact the long-term ozone recovery expected from the Montreal
486 Protocol. In addition, the simulations show no significant sea surface temperature change
487 between the all-forcing runs and the control runs across 10 ensembles until early 2023 (not
488 shown). However, the sustained water vapor enhancement due to HTHH eruption might be
489 expected to affect surface climate in the upcoming years. The HTHH eruption provides a
490 remarkable natural experiment for validating a fully coupled chemistry-climate model and
491 provides confidence in ensemble forecast simulations, such as those performed here.

492

493 **Acknowledgments**

494 This project received funding from NOAA's Earth Radiation Budget (ERB) Initiative (CPO #03-
495 01-07-001). This research was supported in part by NOAA cooperative agreements
496 NA17OAR4320101 and NA22OAR4320151, and by the NASA Aura Science Team under Grant

497 80NSSC20K0928. OBT was supported by NSF Award AGS 1853932. The work contribution of
498 WY was performed under the auspices of the US Department of Energy (DOE) by Lawrence
499 Livermore National Laboratory under contract no. DE-AC52-07NA27344. JZ is supported by
500 the NSF via NCAR's Advanced Study Program Postdoctoral Fellowship. The authors thank Drs
501 Nathaniel Livesey, Michelle Santee, Paul Newman, Holger Vömel, Karen Rosenlof, Robert
502 Portmann, and Ewa Bednarz for helpful discussions. NCAR's Community Earth System Model
503 project is supported primarily by the National Science Foundation. This material is based upon
504 work supported by the National Center for Atmospheric Research, which is a major facility
505 sponsored by the NSF under Cooperative Agreement No. 1852977. Computing and data storage
506 resources, including the Cheyenne supercomputer (doi:10.5065/D6RX99HX), were provided by
507 the Computational and Information Systems Laboratory (CISL) at NCAR.

508

509 **Open Research**

510 ERA5 meteorological products are available from the Copernicus Climate Data Store
511 ([https://cds.climate.copernicus.eu/cdsapp#!/dataset/reanalysis-era5-pressure-](https://cds.climate.copernicus.eu/cdsapp#!/dataset/reanalysis-era5-pressure-levels?tab=form)
512 [levels?tab=form](#)). CESM2/WACCM6 is an open-source community model, which was
513 developed with support primarily from the National Science Foundation. WACCM6 source code
514 can be downloaded at <https://www.cesm.ucar.edu/models/cesm2/download>.

515

516 **References**

517 Andrews, David G, James R Holton, and Conway B Leovy. 1987. *Middle Atmosphere*
518 *Dynamics*. Academic press.
519 Bourassa, Adam E, Daniel J Zawada, Landon A Rieger, Taran W Warnock, Matthew Toohey,

520 and Doug A Degenstein. 2023. "Tomographic Retrievals of Hunga Tonga-Hunga Ha'apai
521 Volcanic Aerosol." *Geophysical Research Letters* 50 (3): e2022GL101978.

522 Carn, Simon, Nickolay Krotkov, Bradford Fisher, and Can Li. 2022. "Out of the Blue: Volcanic
523 SO₂ Emissions during the 2021-2022 Hunga Tonga-Hunga Ha'apai Eruptions."

524 Coy, Lawrence, P A Newman, K Wargan, G Partyka, S E Strahan, and S Pawson. 2022.
525 "Stratospheric Circulation Changes Associated With the Hunga Tonga-Hunga Ha'apai
526 Eruption." *Geophysical Research Letters* 49 (22): e2022GL100982.

527 Gelaro, Ronald, Will McCarty, Max J Suárez, Ricardo Todling, Andrea Molod, Lawrence
528 Takacs, Cynthia A Randles, Anton Darmenov, Michael G Bosilovich, and Rolf Reichle.
529 2017. "The Modern-Era Retrospective Analysis for Research and Applications, Version 2
530 (MERRA-2)." *Journal of Climate* 30 (14): 5419–54.

531 Gettelman, A, M J Mills, D E Kinnison, R R Garcia, A K Smith, D R Marsh, S Tilmes, F Vitt, C
532 G Bardeen, and J McInerny. 2019. "The Whole Atmosphere Community Climate Model
533 Version 6 (WACCM6)." *Journal of Geophysical Research: Atmospheres* 124 (23): 12380–
534 403.

535 Hersbach, Hans, Bill Bell, Paul Berrisford, Shoji Hirahara, András Horányi, Joaquín Muñoz-
536 Sabater, Julien Nicolas, Carole Peubey, Raluca Radu, and Dinand Schepers. 2020. "The
537 ERA5 Global Reanalysis." *Quarterly Journal of the Royal Meteorological Society* 146
538 (730): 1999–2049.

539 Hitchcock, Peter, Theodore G Shepherd, and Shigeo Yoden. 2010. "On the Approximation of
540 Local and Linear Radiative Damping in the Middle Atmosphere." *Journal of the
541 Atmospheric Sciences* 67 (6): 2070–85.

542 Hofmann, David J, and Susan Solomon. 1989. "Ozone Destruction through Heterogeneous

543 Chemistry Following the Eruption of El Chichon.” *Journal of Geophysical Research: Atmospheres* 94 (D4): 5029–41.

544

545 Holton, J. R., & Mass, C. (1976). Stratospheric vacillation cycles. *Journal of Atmospheric Sciences*, 33(11), 2218–2225.

546

547 Jenkins, Stuart, Chris Smith, Myles Allen, and Roy Grainger. 2023. “Tonga Eruption Increases Chance of Temporary Surface Temperature Anomaly above 1.5° C.” *Nature Climate Change*, 1–3.

548

549

550 Khaykin, Sergey, Aurelien Podglajen, Felix Ploeger, Jens Uwe Grooß, Florent Tencé, Slimane Bekki, Konstantin Khlopenkov, Kristopher Bedka, Landon Rieger, and Alexandre Baron. 2022. “Global Perturbation of Stratospheric Water and Aerosol Burden by Hunga

551

552 Eruption.”

553

554 Legras, Bernard, Clair Duchamp, Pasquale Sellitto, Aurélien Podglajen, Elisa Carboni, Richard Siddans, Jens-Uwe Grooß, Sergey Khaykin, and Felix Ploeger. 2022. “The Evolution and Dynamics of the Hunga Tonga–Hunga Ha’apai Sulfate Aerosol Plume in the Stratosphere.” *Atmospheric Chemistry and Physics* 22 (22): 14957–70.

555

556

557

558 Li, Feng, and Paul Newman. 2020. “Stratospheric Water Vapor Feedback and Its Climate Impacts in the Coupled Atmosphere–Ocean Goddard Earth Observing System Chemistry–Climate Model.” *Climate Dynamics* 55 (5): 1585–95.

559

560

561 Livesey, N J, W G Read, P A Wagner, L Froidevaux, M L Santee, and M J Schwartz. 2020. “Version 5.0 x Level 2 and 3 Data Quality and Description Document (Tech. Rep. No. JPL D-105336 Rev. A).” *Jet Propulsion Laboratory*.

562

563

564 Long, C. S., & Stowe, L. L. (1994). Using the NOAA/AVHRR to study stratospheric aerosol optical thicknesses following the Mt. Pinatubo eruption. *Geophysical Research Letters*,

565

566 21(20), 2215–2218.

567 Lu, Jinpeng, Sijia Lou, Xin Huang, Lian Xue, Ke Ding, Tengyu Liu, Yue Ma, Wuke Wang, and
568 Aijun Ding. 2023. “Stratospheric Aerosol and Ozone Responses to the Hunga Tonga-Hunga
569 Ha’apai Volcanic Eruption.” *Geophysical Research Letters* 50 (4): e2022GL102315.

570 Manney, Gloria L, Michelle L Santee, Alyn Lambert, Luis Millan, Ken Minschwaner, Frank
571 Werner, Zachary Duane Lawrence, William G Read, Nathaniel J Livesey, and Tao Wang.
572 2023. “Siege of the South: Hunga Tonga-Hunga Ha’apai Water Vapor Excluded from 2022
573 Antarctic Stratospheric Polar Vortex.” *Authorea Preprints*.

574 Millan, Luis, Michelle L Santee, Alyn Lambert, Nathaniel J Livesey, Frank Werner, Michael J
575 Schwartz, Hugh Charles Pumphrey, Gloria L Manney, Yuan Wang, and Hui Su. 2022. “The
576 Hunga Tonga-Hunga Ha’apai Hydration of the Stratosphere.”

577 Quaglia, I., Timmreck, C., Niemeier, U., Visioni, D., Pitari, G., Brodowsky, C., Brühl, C.,
578 Dhomse, S. S., Franke, H., & Laakso, A. (2023). Interactive stratospheric aerosol models'
579 response to different amounts and altitudes of SO₂ injection during the 1991 Pinatubo
580 eruption. *Atmospheric Chemistry and Physics*, 23(2), 921–948.

581 Randel, William J, Benjamin R Johnston, John J Braun, Sergey Sokolovskiy, Holger Vömel,
582 Aurelien Podglajen, and Bernard Legras. 2023. “Stratospheric Water Vapor from the Hunga
583 Tonga–Hunga Ha’apai Volcanic Eruption Deduced from COSMIC-2 Radio Occultation.”
584 *Remote Sensing* 15 (8): 2167.

585 Randel, W. J., & Newman, P. A. (1998). The stratosphere in the Southern Hemisphere. In
586 *Meteorology of the Southern Hemisphere* (pp. 243–282). Springer.

587 Randel, William J, Fei Wu, Richard Swinbank, John Nash, and Alan O’Neill. 1999. “Global
588 QBO Circulation Derived from UKMO Stratospheric Analyses.” *Journal of the*

589 *Atmospheric Sciences* 56 (4): 457–74.

590 Richter, Jadwiga H, Anne A Glanville, James Edwards, Brian Kauffman, Nicholas A Davis,

591 Abigail Jaye, Hyemi Kim, Nicholas M Pedatella, Lantao Sun, and Judith Berner. 2022.

592 “Subseasonal Earth System Prediction with CESM2.” *Weather and Forecasting* 37 (6):

593 797–815.

594 Rieger, L A, W J Randel, A E Bourassa, and S Solomon. 2021. “Stratospheric Temperature and

595 Ozone Anomalies Associated with the 2020 Australian New Year Fires.” *Geophysical*

596 *Research Letters* 48 (24): e2021GL095898.

597 Santee, M L, A Lambert, G L Manney, N J Livesey, L Froidevaux, J L Neu, M J Schwartz, L F

598 Millán, F Werner, and W G Read. 2022. “Prolonged and Pervasive Perturbations in the

599 Composition of the Southern Hemisphere Midlatitude Lower Stratosphere from the

600 Australian New Year’s Fires.” *Geophysical Research Letters* 49 (4): e2021GL096270.

601 Schoeberl, M R, Yi Wang, R Ueyama, G Taha, E Jensen, and W Yu. 2022. “Analysis and Impact

602 of the Hunga Tonga-Hunga Ha’apai Stratospheric Water Vapor Plume.” *Geophysical*

603 *Research Letters* 49 (20): e2022GL100248.

604 <https://doi.org/https://doi.org/10.1029/2022GL100248>.

605 Schoeberl, M R, Yi Wang, R Ueyama, G Taha, and W Yu. 2023. “The Cross Equatorial

606 Transport of the Hunga Tonga-Hunga Ha’apai Eruption Plume.” *Geophysical Research*

607 *Letters* 50 (4): e2022GL102443. <https://doi.org/https://doi.org/10.1029/2022GL102443>.

608 Solomon, Susan. 1999. “Stratospheric Ozone Depletion: A Review of Concepts and History.”

609 *Reviews of Geophysics* 37 (3): 275–316.

610 Solomon, Susan, Kimberlee Dube, Kane Stone, Pengfei Yu, Doug Kinnison, Owen B Toon,

611 Susan E Strahan, Karen H Rosenlof, Robert Portmann, and Sean Davis. 2022. “On the

612 Stratospheric Chemistry of Midlatitude Wildfire Smoke.” *Proceedings of the National*
613 *Academy of Sciences* 119 (10): e2117325119.

614 Solomon, Susan, Rolando R Garcia, F Sherwood Rowland, and Donald J Wuebbles. 1986. “On
615 the Depletion of Antarctic Ozone.” *Nature* 321 (6072): 755–58.

616 Solomon, Susan, Diane J Ivy, Doug Kinnison, Michael J Mills, Ryan R Neely III, and Anja
617 Schmidt. 2016. “Emergence of Healing in the Antarctic Ozone Layer.” *Science* 353 (6296):
618 269–74.

619 Solomon, Susan, Karen H Rosenlof, Robert W Portmann, John S Daniel, Sean M Davis, Todd J
620 Sanford, and Gian-Kasper Plattner. 2010. “Contributions of Stratospheric Water Vapor to
621 Decadal Changes in the Rate of Global Warming.” *Science* 327 (5970): 1219–23.

622 Solomon, Susan, Kane Stone, Pengfei Yu, D M Murphy, Doug Kinnison, A R Ravishankara, and
623 Peidong Wang. 2023. “Chlorine Activation and Enhanced Ozone Depletion Induced by
624 Wildfire Aerosol.” *Nature* 615 (7951): 259–64.

625 Stone, Kane A, Susan Solomon, Doug E Kinnison, Michael C Pitts, Lamont R Poole, Michael J
626 Mills, Anja Schmidt, Ryan R Neely III, Diane Ivy, and Michael J Schwartz. 2017.
627 “Observing the Impact of Calbuco Volcanic Aerosols on South Polar Ozone Depletion in
628 2015.” *Journal of Geophysical Research: Atmospheres* 122 (21): 11–862.

629 Tie, XueXi, and Guy Brasseur. 1995. “The Response of Stratospheric Ozone to Volcanic
630 Eruptions: Sensitivity to Atmospheric Chlorine Loading.” *Geophysical Research Letters* 22
631 (22): 3035–38.

632 Tilmes, S., Richter, J. H., Mills, M. J., Kravitz, B., MacMartin, D. G., Vitt, F., Tribbia, J. J., &
633 Lamarque, J. (2017). Sensitivity of aerosol distribution and climate response to stratospheric
634 SO₂ injection locations. *Journal of Geophysical Research: Atmospheres*, 122(23), 12–591.

635 Vömel, Holger, Stephanie Evan, and Matt Tully. 2022. "Water Vapor Injection into the
636 Stratosphere by Hunga Tonga-Hunga Ha'apai." *Science* 377 (6613): 1444–47.

637 Waters, Joe W., Lucien Froidevaux, Robert S. Harwood, Robert F. Jarnot, Herbert M. Pickett,
638 William G. Read, Peter H. Siegel et al. "The earth observing system microwave limb
639 sounder (EOS MLS) on the Aura satellite." *IEEE transactions on geoscience and remote
640 sensing* 44, no. 5 (2006): 1075-1092.

641 Yook, Simchan, David W J Thompson, and Susan Solomon. 2022. "Climate Impacts and
642 Potential Drivers of the Unprecedented Antarctic Ozone Holes of 2020 and 2021."
643 *Geophysical Research Letters* 49 (10): e2022GL098064.

644 Yu, W., Garcia, R. R., Yue, J., Smith, A. K., Wang, X., Randel, W. J., Qiao, Z., Zhu, Y., Harvey,
645 V. L., & Tilmes, S. (2023). Mesospheric temperature and circulation response to the Hunga
646 Tonga-Hunga-Ha'apai volcanic eruption. *Authorea Preprints*.

647 Yulaeva, Elena, James R Holton, and John M Wallace. 1994. "On the Cause of the Annual Cycle
648 in Tropical Lower-Stratospheric Temperatures." *Journal of Atmospheric Sciences* 51 (2):
649 169–74.

650 Zhang, J., Kinnison, D. E., Zhu, Y., Wang, X., Tilmes, S., Dubé, K. R., & Randel, W. J. (2023).
651 *Chemistry contribution to stratospheric ozone depletion after the unprecedented water rich
652 Hunga Tonga eruption.*

653

654 Zhu, Yunqian, Charles G Bardeen, Simone Tilmes, Michael J Mills, Xinyue Wang, V Lynn
655 Harvey, Ghassan Taha, Douglas Kinnison, Robert W Portmann, and Pengfei Yu. 2022.
656 "Perturbations in Stratospheric Aerosol Evolution Due to the Water-Rich Plume of the 2022
657 Hunga-Tonga Eruption." *Communications Earth & Environment* 3 (1): 1–7.

658 Zhu, Yunqian, Owen B Toon, Alyn Lambert, Douglas E Kinnison, Charles Bardeen, and
659 Michael C Pitts. 2017. "Development of a Polar Stratospheric Cloud Model within the
660 Community Earth System Model: Assessment of 2010 Antarctic Winter." *Journal of*
661 *Geophysical Research: Atmospheres* 122 (19): 10–418.

662 Zhu, Yunqian, Owen Brian Toon, Douglas Kinnison, V Lynn Harvey, Michael J Mills, Charles
663 G Bardeen, Michael Pitts, Nelson Bègue, Jean-Baptiste Renard, and Gwenaël Berthet. 2018.
664 "Stratospheric Aerosols, Polar Stratospheric Clouds, and Polar Ozone Depletion after the
665 Mount Calbuco Eruption in 2015." *Journal of Geophysical Research: Atmospheres* 123
666 (21): 12–308.

667

668